Multibody Syst Dyn (2014) 31:497–517
DOI 10.1007/s11044-013-9398-z

Combining vibrational linear-by-part dynamics and kinetic-based decoupling of the dynamics for multiple smooth impacts with redundancy

Ana Barjau · Joaquim A. Batlle · Josep M. Font-Llagunes

Received: 27 May 2013 / Accepted: 2 September 2013 / Published online: 3 October 2013

Abstract This article proposes a simple linear-by-part approach for perfectly elastic 3D multiple-point impacts in multibody systems with perfect constraints and no friction, applicable both to nonredundant and redundant cases (where the normal velocities of the contact points are not independent). The approach is based on a vibrational dynamical model, and uses the so called "independent contact space." Two different time and space scales are used. At the macroscale, the impact interval is negligible, and the overall system configuration is assumed to be constant. Consequently, the inertia and Jacobian matrices appearing in the formulation are also constant. The dynamics at the contact points is simulated through stiff springs undergoing very small deformations and generating system vibrations at the microscale. The total impact interval is split into phases, each corresponding to a constant set of compressed springs responsible for an elastic potential energy. For each phase, a reduced inertia matrix associated with a set of contact points, and a reduced stiffness matrix obtained from the potential energy (associated with all contact points undergoing compression) are introduced. From these matrices, a modal analysis is performed yielding an all-analytical solution within each phase. The main difference between the redundant and nonredundant cases concerns the inertia and stiffness matrices for modal analysis. While in the former case, both are related to the total set of contact points (total contact space), in the latter one they are related to two subsets: a subset of independent points for the inertia matrix (independent contact space), and the total set for the stiffness matrix. A second difference concerns the calculation of the normal impulses generated at each contact point. For the nonredundant case, they can be directly obtained from the total incremental normal velocities of the contact points through the inertia and stiffness matrices. For the redundant one, they can be obtained by adding up their incremental values at each impact phase. This requires an

A. Barjau (✉) · J.A. Batlle · J.M. Font-Llagunes
Department of Mechanical Engineering and Biomedical Engineering Research Centre, Universitat Politècnica de Catalunya, Diagonal 647, 08028 Barcelona, Spain
e-mail: ana.barjau@upc.edu

J.A. Batlle
e-mail: agullo.batlle@upc.edu

J.M. Font-Llagunes
e-mail: josep.m.font@upc.edu

updating of a new effective stiffness matrix depending on the contact points undergoing compression at each phase. Four planar application cases are presented involving a single body and a multibody system colliding with a smooth ground.

Keywords Multiple-point impact · Contact dynamics · Modal analysis · Redundancy

1 Introduction

The dynamics of multiple-point impacts in multibody systems is a topic of interest in many different fields. Many publications have been devoted to the subject; nevertheless, it is still open to research.

When the systems undergoing the impact contain flexible parts, the problem is usually studied with a finite-element method [1]. For the case of ideal rigid bodies, the approaches found in literature can be roughly classified into continuous approaches and impulsive ones [2]. In continuous methods, the interactions at the contact points of the colliding systems are described through compliant models, and the equations of motion are solved during the impact interval. The evolution of both the configuration and the velocities of the system are tracked continuously until the end of the impact, which is determined by the system's dynamics. Neither the impact duration nor the system's final mechanical state are known beforehand.

In impulsive methods, as the time interval elapsed between the beginning and the end of the impact is very small (as compared to the time scale of nonimpact or smooth dynamics), the system configuration is assumed to be constant. In some impulsive approaches, the post-impact mechanical state is obtained through integration. For the particular case of single-point impacts, the integration variable can be the normal impulse generated at the impact point [3], and there is no need of a compliant model. The "end condition" (that is, the condition defining the impact end) has to be established beforehand, and it usually takes the form of an algebraic equation relating the preimpact and the post-impact values of a same variable. In all other cases, constitutive models are necessary (linear or nonlinear springs and dampers). The integration variable is either time or the normal impulses at the impact points [4].

When studying impacts in ball chains (a system that has been widely used to test different approaches), the contact model which is most consistent with experimental results is Hertz's contact law. In that case, the equations of motion are nonlinear and have to be solved numerically, and this can be very demanding from the computational point of view.

Linear models are also encountered in literature. Though not as realistic as Hertz's model, the advantage is that they allow some analytical developments yielding interesting and physically consistent results [5–9].

For the particular case of single-point or multiple-point impacts without friction, some impulsive methods treat the impact interval as a "black box": The system evolution within the interval is not explored, and the post-impact mechanical state is obtained from the preimpact one through purely algebraic equations. The unknowns in that case are not only the system final velocities, but also the impulses generated at the contact points. Thus, the equations of motion are insufficient, and they have to be completed with a set of equations, whose number equals that of contact points.

The complementary equations must take the form of end laws (or restitution coefficients) if the "black box" philosophy has to be maintained. Those laws are assumed to be a simple way to take into account the energy loss associated with the deformation at the contact

points. Among them, the three most commonly encountered are Newton's kinematic rule, Poisson's kinetic rule, and the energetic rule [10–15].

The restitution rules relate the post-impact value of a variable to the preimpact one through a restitution coefficient which is supposed to take values constrained in the [0, 1] interval, 1 corresponding to perfect elastic impacts and 0 corresponding to totally plastic ones. Though usually applied in frictionless problems, some authors use them (or on-purpose forms of them) in dissipative collisions (see, for instance, [16]).

For the case of single-point frictionless impacts, the three restitution coefficients are equivalent. However, Newton's and Poisson's coefficient may lead to energetically inconsistent results in rough impacts [17]. For the case of multiple-point frictionless impacts, Newton's and Poisson's rules do not take into account properly the possible coupling effects among the contact points, and thus do not apply in general. As they may lead to energy overestimation, some authors have proposed *ad hoc* methods to avoid that drawback (see, for example, [18]).

The different approaches encountered in the scientific literature to overcome this problem can be classified into two groups: propagation methods and simultaneous ones [19]. In propagation methods, the multiple-point impact is treated as a sequence of single-point impacts without overlapping [20]. However, this assumption may not be fulfilled. Moreover, when it holds, the results are in general sequence-dependent (that is, the system's final mechanical state depends on the particular sequence of single-point collisions assumed in the calculation).

In some simultaneous methods, total overlapping of uncoupled independent impacts is assumed [21]. However, this situation is an exception, as in general coupling cannot be avoided. In other cases, coupling coefficients are introduced to cope with overlapping [22], but their values are not simple to assess. Dynamical coupling among the contact points is the main reason why single-point impact approaches cannot be directly extrapolated to multiple-point ones (as in [4]).

A particularly interesting situation among multiple-point simultaneous impacts is that of redundant impacts. Redundancy is a concept appearing in different situations, and different definitions can be found in the scientific literature. In this paper—which deals with frictionless impacts—redundancy applies to multibody systems where the normal velocities of the contact points are not independent.

The existing rigid-body approaches for simultaneous multiple-point impacts fail in case of redundancy. Though there are a few scientific papers dealing with multiple-point impacts, most of them are related to particular cases where redundancy does not occur. Ruspini and Khatib [19] treat redundant impacts (in the sense mentioned previously). However, their treatment of redundancy does not always apply (as will be explained later on). Johansson [23] solves the indeterminacy of contact forces associated with redundancy by means of mathematical approaches, such as Single Value Decomposition (SVD) that lead to approximate solutions with no clear physical meaning.

The aim of this work is to present a linear-by-part approach to treat redundant multiple-point frictionless impacts simple enough as to allow analytical solutions within the impact interval, but retaining energetic consistency and high sensitivity to initial conditions (that is, a small perturbation in the initial mechanical state yields a completely different final mechanical state), which is a main feature in multiple-point impacts, without need of arbitrary hypotheses concerning impacts sequences or coupling effects. The method can be described as hybrid because, though relying on a linear-by-part stiffness compliant model, analytical vibratory solutions obtained from modal analysis are used, thus allowing a discrete sampling of the impact interval and not a continuous exploration. Though energy dissipation

is not considered in the present work, its implementation (through hysteretic damping or bi-stiffness contact model, for instance) is perfectly compatible with the lossless algorithm proposed here.

Each contact point under compression is modeled through a finite normal linear stiffness (high enough to assume constant configuration at a macro scale throughout the process). At a microscale, the contact points may show a positive or zero normal separation, or a negative one. In the former case, the contact points are called "passive" points and there is no normal stiffness associated with them. In the latter case, the corresponding linear springs undergo compression or expansion processes (depending on the sign of the normal velocities), and the contact points are classified as "active" ones.

If energy dissipation is not considered (as is the case in the present work), the impact interval is split into phases, each one presenting a constant set of active and passive contact points. Transition between phases occurs whenever an active point becomes passive or conversely (passive becoming active).

In order to proceed to modal analysis at each phase, we need appropriate inertia and stiffness matrices. When not colliding (free motion), the inertial properties of the n-Degree-of-Freedom (DoF) multibody system are given by matrix $\mathbf{M}_u(\boldsymbol{q})$ associated with the kinetic energy $T = (1/2)\boldsymbol{u}^T\mathbf{M}_u\boldsymbol{u}$, where $\boldsymbol{u}$ is the vector of the n generalized velocities. The stiffness matrix is obviously zero.

Under impact (constrained motion), a usual practice is to switch from the "DoF space" description to a "contact space" description [24]. In that space, the normal velocities of the contact points $\boldsymbol{v}_n = \dot{\boldsymbol{\delta}}_n$ (where $\boldsymbol{\delta}_n$ are the relative normal displacements at the contact points) are used to describe the multibody system's dynamics. The "contact space" inertia matrix $\mathbf{M}_n$ provides a description of the inertial properties of the system at the contact points, and it is related to the inertia matrix $\mathbf{M}_u$ through

$$\mathbf{M}_n^{-1} = \mathbf{A}\mathbf{M}_u^{-1}\mathbf{A}^T \equiv \mathbf{W}, \tag{1.1}$$

where $\mathbf{A}$ is the Jacobian matrix relating $\boldsymbol{v}_n$ to $\boldsymbol{u}$, $\boldsymbol{v}_n = \mathbf{A}\boldsymbol{u}$. Matrix $\mathbf{W}$ is often called "mechanical compliance" matrix [24] or "Delassus operator" of the system [25].

For the case of nonredundant impacts, the matrix $\mathbf{W}$ is invertible, and the reduced inertia matrix $\mathbf{M}_n$ can be used to calculate the quadratic form $T_n = (1/2)\boldsymbol{v}_n^T\mathbf{M}_n\boldsymbol{v}_n$, called sometimes "pseudo kinetic energy" as it does not coincide with the total kinetic energy in general. However, the kinetic energy change of the system associated with an impact phase is equal to that of T_n [25]:

$$\Delta T]_{\text{phase}} = \Delta T_n]_{\text{phase}}. \tag{1.2}$$

This suggests the use of matrix $\mathbf{M}_n$ as inertia matrix for the modal analysis at each phase in the nonredundant impact.

The stiffness matrix $\mathbf{K}_n$ is related to the potential elastic energy U associated with the linear springs undergoing deformation, which can be calculated through

$$U = \frac{1}{2}\boldsymbol{\delta}_n^T\mathbf{K}_n\boldsymbol{\delta}_n. \tag{1.3}$$

Matrix $\mathbf{K}_n$ is strictly diagonal with elements $k_j > 0$ if there is indentation (that is, $\delta_{nj} < 0$) at the contact point Q_j, and $k_j = 0$ otherwise. The eigenvalues and eigenvectors of the dynamical matrix $\mathbf{D} \equiv \mathbf{M}_n^{-1}\mathbf{K}_n$ define the eigenfrequencies and eigenmodes of the vibration problem.

The phase initial velocities are projected on the modal solutions, and the normal displacements and velocities of all the contact points (both active and passive) are then expressed

analytically as a superposition of modes. The time instant corresponding to a transition to a new phase is then determined. In general, this calls for the resolution of transcendental equations. The final state of the contact points is obtained from the modal solutions at that transition time instant. The impact is over when all the contact points are passive and show a positive normal separation velocity.

In this approach, the impact overlapping (that is, the simultaneous existence of several active points) and the coupling between contact points appear directly as a consequence of the system dynamics. From the mathematical point of view, coupling is related to the off-diagonal elements in $\mathbf{W}$.

In redundant impacts, the compliance matrix $\mathbf{W}$ is not invertible. To overcome this situation, Ruspini and Khatib [19, 24] propose a reduction of the contact space to that of just the active points (which are in general a subset of the contact points), so that the compliance matrix becomes:

$$\tilde{\mathbf{W}} = \mathbf{A}_{\text{act}} \mathbf{M}_u^{-1} \mathbf{A}_{\text{act}}^T, \tag{1.4}$$

and then proceed to its inversion to obtain the "active contact space" inertia matrix $\tilde{\mathbf{M}}_n$. However, the active points may not be independent in general, and thus $\tilde{\mathbf{W}}$ may not be invertible.

Instead of reducing the "contact space" dimension, Constantinescu et al. [27] use a generalized inverse (or pseudo-inverse) of $\tilde{\mathbf{W}}$ (though they do not specify which sort of pseudo-inverse), which yields only an approximate solution.

Our approach is based on the use of an "independent contact space" inertia matrix $\mathbf{M}_{n,\text{ind}}$ associated with a set of independent points (redundant points must be excluded) no matter their colliding state (active or passive). Consequently, the stiffness matrix to be used in the modal analysis has to relate the elastic energy to the normal displacements in that independent contact space:

$$U = \frac{1}{2} \boldsymbol{\delta}_{n,\text{ind}}^T \hat{\mathbf{K}}_n \boldsymbol{\delta}_{n,\text{ind}}. \tag{1.5}$$

However, that elastic energy is related to all the active contact points (whether independent or not), and this makes its formulation less straightforward than that of the inertia matrix $\mathbf{M}_{n,\text{ind}}$ (as will be shown in Sect. 4).

Even if all active contact points are independent, our approach is more general than that of Ruspini and Khatib [19, 24], and that of Constantinescu et al. [27]. More precisely, these authors assume implicitly that impact is over simultaneously at all active points, and use Newton's restitution coefficient to relate their post-impact normal velocities to the preimpact ones. This seems to be a usual practice in the field of robotics and haptic simulation and, though probably acceptable for their purposes, we consider that it is not consistent from a physical point of view. In our approach, no assumption is done concerning the impacts end. Moreover, our formulation allows the use of different stiffnesses at the different contact points.

Modal analysis has already been used in impact dynamics. In some cases, to study wave propagation phenomena triggered by the impact [1]; in other cases, just as a tool interesting to explore two-point impacts in ball chain systems [6, 7], but not in a general multibody case and in a systematic way. The main point of our work, however, is that of proposing a physically consistent approach to treat the general case of redundant impacts, something that has not been treated at all in rigid body approaches.

The present article is structured as follows. A brief reminder of the formulation of the impact mechanics Lagrange equations for a multibody system is outlined in Sect. 2. Then the hybrid approach is presented in Sect. 3 for systems in which the colliding points do no present redundancy. The extension to the redundant case is explained in Sects. 4 and 5.

Four application examples are analyzed in Sect. 6, all corresponding to planar motions. The hybrid approach is totally general, and no particular assumption about the space dimensions and number of DoF has been done. Thus, any multibody system undergoing collisions in a 3D space may be treated through our approach. However, we have chosen 2D examples because they can be easily analyzed and validated.

The first two consist on a rigid rod colliding with a smooth surface. Special attention is paid to the sensitivity of the system to perturbations on its configuration. The third and the fourth examples deal with a simple multibody system consisting of a two-link chain (two rigid rods connected by a hinge joint). Section 7 is devoted to conclusions.

2 Lagrange formulation for the nonredundant impact problem

Let us consider an n DoF multibody system, described by the n vector of generalized velocities $\boldsymbol{u}$, undergoing a simultaneous impact at m contact points Q_j. The m normal separation velocities at those contact points $\boldsymbol{v}_n$ (with $m < n$) are related to the generalized velocities $\boldsymbol{u}$ through an $m \times n$ Jacobian matrix of kinematic coefficients, $\boldsymbol{v}_n = \mathbf{A}\boldsymbol{u}$. We will consider first that the m normal velocities are independent, and consequently, $\mathrm{rank}(\mathbf{A}) = m$. The Lagrangian formulation of the system's impact dynamics is

$$\mathbf{M}_u \Delta \boldsymbol{u} = \boldsymbol{\Pi}_u, \tag{2.1}$$

where $\mathbf{M}_u$ is the $n \times n$ inertia matrix for the impact configuration, and $\boldsymbol{\Pi}_u$ is the vector of generalized normal impulses. The n vector $\boldsymbol{\Pi}_u$ is related to the m vector $\boldsymbol{P}_n$ of normal impulses at the contact points through $\boldsymbol{\Pi}_u = \mathbf{A}^T \boldsymbol{P}_n$. The incremental changes $\Delta \boldsymbol{u} = \boldsymbol{u}^+ - \boldsymbol{u}^-$ and $\Delta \boldsymbol{v}_n = \boldsymbol{v}_n^+ - \boldsymbol{v}_n^-$ (where the $(+)$ and $(-)$ indexes stand for "just after" and "just before" impact) are related to the normal impulses $\boldsymbol{P}_n$ through

$$\Delta \boldsymbol{u} = \mathbf{M}_u^{-1} \mathbf{A}^T \boldsymbol{P}_n \quad \text{and} \quad \Delta \boldsymbol{v}_n = \mathbf{A}\mathbf{M}_u^{-1} \mathbf{A}^T \boldsymbol{P}_n. \tag{2.2}$$

In nonredundant cases, $\mathrm{rank}(\mathbf{A}) = m$, and the compliance matrix $\mathbf{W} = \mathbf{A}\mathbf{M}_u^{-1}\mathbf{A}^T$ is a symmetrical and positive definite $m \times m$ matrix, and can be inverted. Accordingly, there exists a biunique relationship between $\Delta \boldsymbol{v}_n$ and $\boldsymbol{P}_n$. Thus, if vector $\Delta \boldsymbol{v}_n$ is known, $\boldsymbol{P}_n$ and the associated $\Delta \boldsymbol{u}$ can be calculated as

$$\boldsymbol{P}_n = \left(\mathbf{A}\mathbf{M}_u^{-1}\mathbf{A}^T\right)^{-1} \Delta \boldsymbol{v}_n \quad \text{and} \quad \Delta \boldsymbol{u} = \mathbf{M}_u^{-1}\mathbf{A}^T \left(\mathbf{A}\mathbf{M}_u^{-1}\mathbf{A}^T\right)^{-1} \Delta \boldsymbol{v}_n, \tag{2.3}$$

and the kinetic energy change as

$$\Delta \boldsymbol{T} = \frac{1}{2}\left(\boldsymbol{u}^+\right)^T \mathbf{M}_u \boldsymbol{u}^+ - \frac{1}{2}\left(\boldsymbol{u}^-\right)^T \mathbf{M}_u \boldsymbol{u}^-. \tag{2.4}$$

The whole problem can be formulated in a more compact way through the use of the $n \times n$ matrix $\mathbf{H}_c$ associated with the decomposition of the kinetic energy for unilaterally-constrained multibody systems [14, 26]:

$$\mathbf{H}_c = \mathbf{M}_u^{-1}\mathbf{A}^T \left(\mathbf{A}\mathbf{M}_u^{-1}\mathbf{A}^T\right)^{-1} \mathbf{A}. \tag{2.5}$$

Matrix $\mathbf{H}_c$ and its complementary $\mathbf{H}_a = (\mathbf{I} - \mathbf{H}_c)$ (with $\mathbf{I} = n \times n$ identity matrix) are idempotent matrices hence projectors. They decompose the generalized velocity vector $\boldsymbol{u}$ into two components, $\boldsymbol{u} = \boldsymbol{u}_c + \boldsymbol{u}_a$, with $\boldsymbol{u}_c = \mathbf{H}_c \boldsymbol{u}$ and $\boldsymbol{u}_a = (\mathbf{I} - \mathbf{H}_c)\boldsymbol{u}$, associated with the spaces of constrained and admissible motions, respectively. An interesting point is that the incremental changes of $\Delta \boldsymbol{u}_c$ and $\Delta \boldsymbol{u}$ due to the impact relate to $\Delta \boldsymbol{v}_n$ exactly in the same way. In other words, $\Delta \boldsymbol{u}_c = \Delta \boldsymbol{u}$ though $\boldsymbol{u}_c \neq \boldsymbol{u}$:

$$\Delta \boldsymbol{u}_c = \mathbf{H}_c \Delta \boldsymbol{u} = \mathbf{M}_u^{-1}\mathbf{A}^T \left(\mathbf{A}\mathbf{M}_u^{-1}\mathbf{A}^T\right)^{-1} \mathbf{A} \Delta \boldsymbol{u} = \mathbf{M}_u^{-1}\mathbf{A}^T \left(\mathbf{A}\mathbf{M}_u^{-1}\mathbf{A}^T\right)^{-1} \Delta \boldsymbol{v}_n. \tag{2.6}$$

The subspaces associated with $\boldsymbol{u}_c$ and $\boldsymbol{u}_a$ are orthogonal through the inertia matrix, and so the kinetic energy can be split into kinetic energy associated with the constrained motion and that associated with admissible motion:

$$T = T_c + T_a = (1/2)\boldsymbol{u}_c^T \mathbf{M}_u \boldsymbol{u}_c + (1/2)\boldsymbol{u}_a^T \mathbf{M}_u \boldsymbol{u}_a. \tag{2.7}$$

As $\Delta\boldsymbol{u} = \Delta\boldsymbol{u}_c$, there are no incremental changes associated with $\boldsymbol{u}_a$ ($\Delta\boldsymbol{u}_a = 0$). Thus, the total kinetic energy change ΔT is only associated to that of T_c, $\Delta T = \Delta T_c$. Moreover, it is easy to prove that

$$T_c = (1/2)\boldsymbol{u}_c^T \mathbf{M}_u \boldsymbol{u}_c = (1/2)\boldsymbol{v}_n^T \left(\mathbf{A}\mathbf{M}_u^{-1}\mathbf{A}^T\right)^{-1} \boldsymbol{v}_n \equiv (1/2)\boldsymbol{v}_n^T \mathbf{M}_n \boldsymbol{v}_n. \tag{2.8}$$

Equation (2.8) suggests that the impact problem can be formulated in a reduced way (that is, can be brought to a lower dimension) through an $m \times m$ reduced inertia matrix associated with the normal velocities at the contact points $\boldsymbol{v}_n$:

$$\mathbf{M}_n \equiv \left(\mathbf{A}\mathbf{M}_u^{-1}\mathbf{A}^T\right)^{-1}. \tag{2.9}$$

This reduction is the starting point of the linear model associated with the contact points presented in the following section.

3 Formulation of the linear model for elastic impacts without redundancy

For impacts without redundancy, the formulation of the impact problem through the contact points is given by:

$$\mathbf{M}_n \Delta\boldsymbol{v}_n = \boldsymbol{P}_n. \tag{3.1}$$

This equation can be solved using a compliant model of the normal contact forces $\boldsymbol{f}_n$ generating the impulses $\boldsymbol{P}_n$. If dissipation is neglected, the usual models found in literature are proportional to a power of the indentation ($\delta_{nj} < 0$):

$$f_n(\mathrm{Q}_j) \equiv f_{nj} = k_j |\delta_{nj}|^{\nu}, \quad \text{with } \delta_{nj} < 0, \tag{3.2}$$

where k_j and δ_{nj} are the stiffness and the normal displacement at the contact point Q_j. When the colliding bodies have nonconforming surfaces, the contact geometry satisfies Hertz theory basic assumptions, and then the nonlinear Hertz model ($\nu = 3/2$) shows good agreement with experimental results.

If elastic constraints with stiffness constant k_j are assumed at the impact points, an m DoF linear vibration problem may be formulated by means of the reduced inertia matrix $\mathbf{M}_n$ and a diagonal stiffness matrix $\mathbf{K}_n$ with elements $k_j > 0$ if there is indentation (that is, $\delta_{nj} < 0$) at the contact point Q_j, and $k_j = 0$ otherwise. The eigenvalues and eigenvectors of the dynamical matrix $\mathbf{D} \equiv \mathbf{M}_n^{-1}\mathbf{K}_n$ define the eigenfrequencies and eigenmodes of the vibration problem.

Coupling effects between contact points are visible in the reduced inertia matrix $\mathbf{M}_n$, but not in the stiffness matrix, and they are associated with its off-diagonal terms.

The active contact points Q_j, under compression, and thus generating nonzero contact forces $\boldsymbol{f}_n$, may change along the impact process. If $\delta_{nj} < 0$ and $\delta_{nj} = 0$ are associated with contact with and without spring compression at point Q_j, respectively, the set of active points changes when:

- $\delta_{nj} = 0$ and $v_{nj} = \dot{\delta}_{nj} > 0$ (end of impact at point Q_j : Q_j has become a passive point)
- $\delta_{ni} = 0$ and $v_{ni} = \dot{\delta}_{ni} < 0$ (starting impact at point Q_i : Q_i is turning to active point)

The impact interval can be split into phases where the set of active points does not change. A new phase starts whenever at least a new impact starts or an impact that has been going on comes to an end (or, what is equivalent, an active point becomes passive, or conversely).

Whenever there is a change in the set of active points, $\mathbf{K}_n$ is changed accordingly (though $\mathbf{M}_n$ remains the same), and the eigenmodes and eigenvalues are recalculated. The initial conditions for the new phase are the final ones of the preceding phase. The impact problem is over when $v_{nj} > 0$ and $\delta_{nj} \geq 0$ at all contact points. The total change of the system generalized velocities $\Delta\boldsymbol{u}$, can be obtained from that of the normal velocities $\Delta\boldsymbol{v}_n$ through Eq. (2.3).

4 Extension to elastic impacts with redundancy

When the m contact points are not independent, $\text{rank}(\mathbf{A}) < m$, and matrix $(\mathbf{A}\mathbf{M}_u^{-1}\mathbf{A}^T)$ cannot be inverted. Thus, Eqs. (2.3) to (2.9) do not apply in the redundant case.

The linear model outlined in the previous section can be extended to the case where the m normal velocities $\boldsymbol{v}_n$ at the contact points are not independent (and so $\text{rank}(\mathbf{A}) = s < m$). In that case, it is always possible to choose a set of $(m - s)$ redundant normal velocities $\boldsymbol{v}_{n,\text{red}} = \mathbf{A}_{\text{red}}\boldsymbol{u}$ and relate them linearly to the set of independent ones $\boldsymbol{v}_{n,\text{ind}} = \mathbf{A}_{\text{ind}}\boldsymbol{u}$ through a $(m - s) \times s$ matrix $\mathbf{R}$ (called "redundancy matrix" from now on):

$$\boldsymbol{v}_{n,\text{red}} = \mathbf{R}\boldsymbol{v}_{n,\text{ind}} = \mathbf{R}\mathbf{A}_{\text{ind}}\boldsymbol{u} \Rightarrow \mathbf{A}_{\text{red}} = \mathbf{R}\mathbf{A}_{\text{ind}}. \tag{4.1}$$

Matrix $\mathbf{R}$ can be calculated analytically from the system's configuration. Once the independent velocities $\boldsymbol{v}_{n,\text{ind}}$ have been chosen, the percussive Lagrange equations can be written as

$$\mathbf{M}_u\Delta\boldsymbol{u} = \mathbf{A}_{\text{ind}}^T\boldsymbol{P}_{n,\text{ind}} + \mathbf{A}_{\text{red}}^T\boldsymbol{P}_{n,\text{red}} = \mathbf{A}_{\text{ind}}^T\left(\boldsymbol{P}_{n,\text{ind}} + \mathbf{R}^T\boldsymbol{P}_{n,\text{red}}\right) \equiv \mathbf{A}_{\text{ind}}^T\boldsymbol{\Pi}_{\text{ind}}, \tag{4.2}$$

and the reduced inertia matrix, associated now with the independent normal velocities, is obtained as in the nonredundant case (though using matrix $\mathbf{A}_{\text{ind}}$ instead of $\mathbf{A}$):

$$\boldsymbol{v}_{n,\text{ind}} = \mathbf{A}_{\text{ind}}\boldsymbol{u} \Rightarrow \mathbf{M}_{n,\text{ind}} \equiv \left(\mathbf{A}_{\text{ind}}\mathbf{M}_u^{-1}\mathbf{A}_{\text{ind}}^T\right)^{-1}. \tag{4.3}$$

Combination of Eqs. (4.2) and (4.3) allows the calculation of vector $\boldsymbol{\Pi}_{\text{ind}}$:

$$\boldsymbol{\Pi}_{\text{ind}} = \left(\mathbf{A}_{\text{ind}}\mathbf{M}_u^{-1}\mathbf{A}_{\text{ind}}^T\right)^{-1}\Delta\boldsymbol{v}_{n,\text{ind}} = \mathbf{M}_{n,\text{ind}}\Delta\boldsymbol{v}_{n,\text{ind}}. \tag{4.4}$$

Though the right-hand side in Eq. (4.4) is only related to the velocities of the independent points, the components of $\boldsymbol{\Pi}_{\text{ind}}$ are not the individual consequence of the compressions generated at the independent contact points as the redundant ones also undergo compression in general (Eq. (4.2)).

The stiffness matrix $\hat{\mathbf{K}}_n$ needed to formulate the vibration problem, however, shows important differences as compared to the nonredundant case, and its calculation is less straightforward. Matrix $\hat{\mathbf{K}}_n$ has to relate the elastic potential energy to the normal displacements $\boldsymbol{\delta}_{n,\text{ind}}$ at the independent contact points. However, a fraction of this energy is associated with the normal displacements at the redundant points $\boldsymbol{\delta}_{n,\text{red}} = \mathbf{R}\boldsymbol{\delta}_{n,\text{ind}}$. The total elastic energy is

$$\begin{aligned} U &= \frac{1}{2}\left(\boldsymbol{\delta}_{n,\text{ind}}^T\mathbf{K}_{\text{ind}}\boldsymbol{\delta}_{n,\text{ind}} + \boldsymbol{\delta}_{n,\text{red}}^T\mathbf{K}_{\text{red}}\boldsymbol{\delta}_{n,\text{red}}\right) \\ &= \frac{1}{2}\boldsymbol{\delta}_{n,\text{ind}}^T\left(\mathbf{K}_{\text{ind}} + \mathbf{R}^T\mathbf{K}_{\text{red}}\mathbf{R}\right)\boldsymbol{\delta}_{n,\text{ind}} \equiv \frac{1}{2}\boldsymbol{\delta}_{n,\text{ind}}^T\hat{\mathbf{K}}_n\boldsymbol{\delta}_{n,\text{ind}}. \end{aligned} \tag{4.5}$$

Thus, the stiffness matrix to be used in the vibrational formulation is $\hat{\mathbf{K}}_n = \mathbf{K}_{\text{ind}} + \mathbf{R}^T \mathbf{K}_{\text{red}} \mathbf{R}$. Matrices $\mathbf{K}_{\text{ind}}$ and $\mathbf{K}_{\text{red}}$ are diagonal and their elements are equal to $k_j > 0$ if point Q_j is active and $k_j = 0$ otherwise. However, $\hat{\mathbf{K}}_n$ is not diagonal in principle. Thus, coupling effects among contact points come not only from the reduced inertia matrix, but also from the stiffness matrix. As mentioned before, matrix $\mathbf{M}_{n,\text{ind}}$ is invariant along the impact interval while $\hat{\mathbf{K}}_n$ changes from phase to phase.

Of course, the particular structure of matrices $\mathbf{R}$, $\mathbf{M}_{n,\text{ind}}$ and $\hat{\mathbf{K}}_n$ depends on the choice of independent points. However, when applied to solve any particular problem, the solution is unique, and does not depend on that choice.

5 Calculation of the individual normal impulses associated with the contact points in redundant cases

The calculation of the normal impulses $\boldsymbol{P}_n$ at the contact points in the redundant case deserves a thorough analysis. In the nonredundant case, they could be obtained from the incremental changes of the normal velocities $\Delta \boldsymbol{v}_n$ through Eq. (3.1). In the redundant case, however, what is directly obtained from the incremental changes of the normal velocities $\Delta \boldsymbol{v}_n$ through Eq. (4.4) is $\boldsymbol{\Pi}_{\text{ind}}$, and not the individual normal impulses P_{nj} at the contact points Q_j.

As the linear model yields the time-evolution of all the normal displacements $\delta_{nj}(t)$ during the impact (directly from the vibration problem if point Q_j belongs to the independent set, or obtained through the redundancy matrix if it is a redundant point), the individual normal impulses P_{nj} at each contact point Q_j can be calculated through time integration:

$$P_{nj} = \int_{-}^{+} f_{nj}(t)\, dt = \int_{-}^{+} k_j \left|\delta_{nj}(t)\right| dt. \tag{5.1}$$

This integration does not fit the general philosophy of the present approach, which is based on algebraic equations and analytical solutions. However, there is an alternative method, perfectly matching this algebraic point of view, to calculate the individual P_{nj} without need of integration. The general idea is to obtain the total impulse P_{nj} developed at each contact point Q_j from its incremental value for each impact phase once the vibration problem has been solved:

$$P_{nj} = \sum_{ph} [\Delta P_{nj}]_{ph} \tag{5.2}$$

For each phase within the impact interval, the vibrational problem gives the colliding state (active/passive) of each contact point, the incremental value of the generalized velocities $[\Delta \boldsymbol{u}]_{ph}$ and that of the generalized impulses $[\Delta \boldsymbol{\Pi}]_{ph}$,

$$\mathbf{M}_u [\Delta \boldsymbol{u}]_{ph} = [\Delta \boldsymbol{\Pi}_u]_{ph}. \tag{5.3}$$

If point Q_j is passive during phase ph, the corresponding ΔP_{nj} in that phase is zero, and does not contribute to the value of $[\Delta \boldsymbol{\Pi}_u]_{ph}$. If it is active, $\Delta P_{nj} > 0$ and its value is associated with the contact force f_{nj} developed at that point, which depends directly on the corresponding normal displacement δ_{nj}.

Thus, as far as the calculation of individual normal impulses is concerned, passive points can be totally disregarded. Defining the Jacobian matrix relating the normal velocities of the active points to the generalized one within a phase:

$$\boldsymbol{v}_{n,\text{act}}]_{ph} = \mathbf{A}_{\text{act}}]_{ph} \boldsymbol{u}, \tag{5.4}$$

and combining it with Eq. (5.3) yields

$$\mathbf{M}_u[\Delta \boldsymbol{u}]_{ph} = \mathbf{A}^T_{n,\mathrm{act}} \Delta \boldsymbol{P}_{n,\mathrm{act}}]_{ph} \Rightarrow \Delta \boldsymbol{v}_{n,\mathrm{act}}]_{ph} = \left(\mathbf{A}_{\mathrm{act}} \mathbf{M}_u^{-1} \mathbf{A}^T_{\mathrm{act}}\right) \Delta \boldsymbol{P}_{n,\mathrm{act}}]_{ph}. \tag{5.5}$$

If all the active points within that phase are independent, matrix $(\mathbf{A}_{\mathrm{act}} \mathbf{M}_u^{-1} \mathbf{A}^T_{\mathrm{act}})$ is invertible, and the individual impulses are obtained straightaway:

$$\Delta \boldsymbol{P}_{n,\mathrm{act}}]_{ph} = \left(\mathbf{A}_{\mathrm{act}} \mathbf{M}_u^{-1} \mathbf{A}^T_{\mathrm{act}}\right)^{-1} \Delta \boldsymbol{v}_{n,\mathrm{act}}]_{ph}. \tag{5.6}$$

If this is not the case, the set of active points has to be split into two subsets, one with the active independent points $\mathrm{Q}^{\mathrm{ind}}_{j,\mathrm{act}}$ and the other one with the active dependent ones $\mathrm{Q}^{\mathrm{dep}}_{j,\mathrm{act}}$ (note that these subsets do not coincide in principle with the independent/redundant subsets defined in the vibratory formulation, as they only contain active points). Equation (5.3) can be reformulated as

$$\mathbf{M}_u[\Delta \boldsymbol{u}]_{ph} = \left(\mathbf{A}^{\mathrm{ind}}_{\mathrm{act}}\right)^T \Delta \boldsymbol{P}^{\mathrm{ind}}_{n,\mathrm{act}}\Big]_{ph} + \left(\mathbf{A}^{\mathrm{dep}}_{\mathrm{act}}\right)^T \Delta \boldsymbol{P}^{\mathrm{dep}}_{n,\mathrm{act}}\Big]_{ph}, \tag{5.7}$$

where $\mathbf{A}^{\mathrm{ind}}_{\mathrm{act},ph}$ and $\mathbf{A}^{\mathrm{dep}}_{\mathrm{act},ph}$ are the Jacobian matrices relating the normal velocities of the independent/dependent active points with the generalized velocities during that phase:

$$\boldsymbol{v}^{\mathrm{ind}}_{n,\mathrm{act}}\Big]_{ph} = \mathbf{A}^{\mathrm{ind}}_{\mathrm{act}}\Big]_{ph} \boldsymbol{u}, \qquad \boldsymbol{v}^{\mathrm{dep}}_{n,\mathrm{act}}\Big]_{ph} = \mathbf{A}^{\mathrm{dep}}_{\mathrm{act}}\Big]_{ph} \boldsymbol{u}. \tag{5.8}$$

Finally, a third matrix is introduced which relates the independent and the dependent points velocities (not to be confused with the redundancy matrix $\mathbf{R}$ appearing in the vibratory formulation):

$$\boldsymbol{v}^{\mathrm{dep}}_{n,\mathrm{act}}\Big]_{ph} = \mathbf{R}_{\mathrm{act}} \boldsymbol{v}^{\mathrm{ind}}_{n,\mathrm{act}}\Big]_{ph} \Rightarrow \mathbf{A}^{\mathrm{dep}}_{\mathrm{act}}]_{ph} = \mathbf{R}_{\mathrm{act}} \mathbf{A}^{\mathrm{ind}}_{\mathrm{act}}]_{ph}. \tag{5.9}$$

Matrix $\mathbf{R}_{\mathrm{act},ph}$ is not in general a submatrix of matrix $\mathbf{R}$ in Eq. (4.1) as, according to what has been pointed out recently, the subset of independent points in this calculation does not coincide in principle to that of the vibratory formulation. Combining Eq. (5.9) with Eq. (5.7) yields

$$\begin{aligned} \Delta \boldsymbol{v}^{\mathrm{ind}}_{n,\mathrm{act}}\Big]_{ph} &= \mathbf{A}^{\mathrm{ind}}_{\mathrm{act}} \mathbf{M}_u^{-1} \left(\mathbf{A}^{\mathrm{ind}}_{\mathrm{act}}\right)^T \left(\Delta \boldsymbol{P}^{\mathrm{ind}}_{n,\mathrm{act}} + \mathbf{R}^T_{\mathrm{act},ph} \Delta \boldsymbol{P}^{\mathrm{dep}}_{n,\mathrm{act}}\right)\Big]_{ph} \\ &\equiv \mathbf{M}^{-1}_{\mathrm{ind}} \Delta \boldsymbol{\Pi}_{n,\mathrm{act}}\Big]_{ph}. \end{aligned} \tag{5.10}$$

The normal impulses in Eq. (5.10) are the time integral of the normal forces at the independent and dependent active points during phase ph, $\boldsymbol{f}^{\mathrm{ind}}_{n,\mathrm{act}}(t)$ and $\boldsymbol{f}^{\mathrm{dep}}_{n,\mathrm{act}}(t)$, respectively. They are related to vectors $\boldsymbol{\delta}^{\mathrm{ind}}_{n,\mathrm{act}}(t)$ and $\boldsymbol{\delta}^{\mathrm{dep}}_{n,\mathrm{act}}(t)$ through the stiffness matrices $\mathbf{K}_{\mathrm{ind},ph}$ and $\mathbf{K}_{\mathrm{dep},ph}$ containing the stiffness coefficients at those points (note that all elements in the diagonals of these matrices are positive, as we are only dealing with active points). The generalized contact force $\boldsymbol{F}_{n,\mathrm{act}}(t)$ whose time integral yields the incremental $\Delta \boldsymbol{\Pi}_{n,\mathrm{act}}]_{ph}$ is then

$$\begin{aligned} \boldsymbol{F}_{n,\mathrm{act}}(t) &= \mathbf{K}_{\mathrm{ind}} \boldsymbol{\delta}^{\mathrm{ind}}_{n,\mathrm{act}}(t)\Big]_{ph} + \mathbf{R}^T_{\mathrm{act}} \mathbf{K}_{\mathrm{dep}} \boldsymbol{\delta}^{\mathrm{dep}}_{n,\mathrm{act}}(t)\Big]_{ph} \\ &= \left(\mathbf{K}_{\mathrm{ind}} + \mathbf{R}^T_{\mathrm{act}} \mathbf{K}_{\mathrm{dep}} \mathbf{R}_{\mathrm{act}}\right) \boldsymbol{\delta}^{\mathrm{ind}}_{n,\mathrm{act}}(t)\Big]_{ph} \equiv \mathbf{K}_{\mathrm{act}} \boldsymbol{\delta}^{\mathrm{ind}}_{n,\mathrm{act}}(t)\Big]_{ph}. \end{aligned} \tag{5.11}$$

The structure of the matrix $\mathbf{K}_{\mathrm{act},ph}$ guarantees its invertibility, thus

$$\begin{aligned} \boldsymbol{f}^{\mathrm{ind}}_{n,\mathrm{act}}(t)\Big]_{ph} &= \mathbf{K}_{\mathrm{ind}} \boldsymbol{\delta}^{\mathrm{ind}}_{n,\mathrm{act}}(t)\Big]_{ph} = \mathbf{K}_{\mathrm{ind}} \mathbf{K}^{-1}_{\mathrm{act}} \boldsymbol{F}_{n,\mathrm{act}}(t)\Big]_{ph}, \\ \boldsymbol{f}^{\mathrm{dep}}_{n,\mathrm{act}}(t)\Big]_{ph} &= \mathbf{K}_{\mathrm{dep}} \boldsymbol{\delta}^{\mathrm{dep}}_{n,\mathrm{act}}(t)\Big]_{ph} = \mathbf{K}_{\mathrm{dep}} \mathbf{R}_{\mathrm{act}} \mathbf{K}^{-1}_{\mathrm{act}} \boldsymbol{F}_{n,\mathrm{act}}(t)\Big]_{ph}. \end{aligned} \tag{5.12}$$

Time integration of Eq. (5.12) along the phase ph leads to the incremental values $\Delta \boldsymbol{P}^{\mathrm{ind}}_{n,\mathrm{act}}]_{ph}$ and $\Delta \boldsymbol{P}^{\mathrm{dep}}_{n,\mathrm{act}}]_{ph}$ of the impulses at the active points:

$$\begin{aligned} \Delta \boldsymbol{P}^{\mathrm{ind}}_{n,\mathrm{act}}\Big]_{ph} &= \mathbf{K}_{\mathrm{ind}} \mathbf{K}^{-1}_{\mathrm{act}} \Delta \boldsymbol{\Pi}_n\Big]_{ph}, \\ \Delta \boldsymbol{P}^{\mathrm{dep}}_{n,\mathrm{act}}\Big]_{ph} &= \mathbf{K}_{\mathrm{dep}} \mathbf{R}_{\mathrm{act}} \mathbf{K}^{-1}_{\mathrm{act}} \Delta \boldsymbol{\Pi}_{n,\mathrm{act}}\Big]_{ph}. \end{aligned} \tag{5.13}$$

All the matrices appearing in the previous expressions have to be updated at each phase.

The individual normal impulses for the whole impact process are obtained by adding up the increments given by Eq. (5.13) for the successive phases. Note that any particular point, when in active state, may belong to the independent subset in some phases and to the dependent one in some others.

6 Application examples

Four application examples with planar motion have been considered: a two-point and a five-point impact of a single rigid body system, and a three-point and six-point impact of a two-link chain. In all cases, different initial states have been explored in order to illustrate the sensitivity to the initial conditions, a main feature in multiple-point impact problems. The particular value of the springs stiffness has been chosen high enough as to yield sufficiently small normal displacements compatible with the condition of "constant configuration" (assumed throughout the simulation).

It is worth pointing out that a simultaneous multiple-point collision of a rod with a flat surface (which is the case of the first two application examples) cannot be described just as a line-to-line impact, as the result depends on the number and particular location of the impact points (as will be seen in the following examples).

6.1 Example I: two-point frictionless impact of a single rigid body

The first example consists on a two-point impact of a rod on a fixed ground (Fig. 1). The mass is concentrated on half of its length, and the contact points Q_1 and Q_2 are located at the rod ends. The generalized velocities are shown in Fig. 1, and correspond to the horizontal and vertical velocities of the center of mass, and the rod angular velocity. As the two normal velocities are independent, there is no redundancy.

A first case has been explored in order to choose suitable stiffness values. Figure 2 corresponds to a simultaneous impact with initial pure vertical downwards translation, and same k values $k_1 = k_2 = 10^8$ N/m. The resulting indentations at both colliding points are sufficiently small (a few μm) as not to invalidate the assumption of constant configuration (in the time macroscale).

Of course, the stiffer the springs, the shorter the impact duration and the lower the indentations. However, the generalized velocities (DoF, Fig. 2(c)) and the normal separating

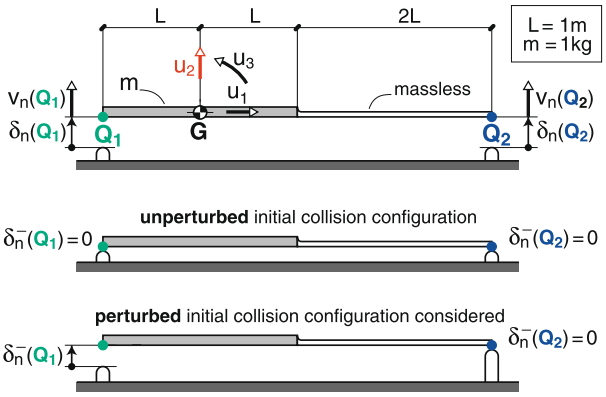

Fig. 1 Two-point impact of a rod with a fixed ground

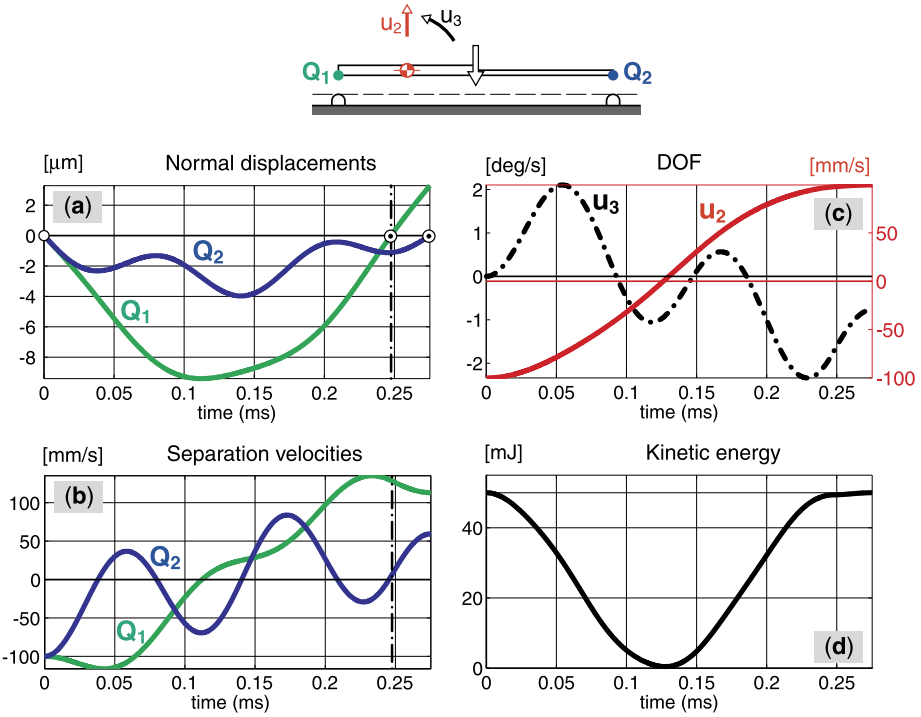

Fig. 2 Evolution of (**a**) $\boldsymbol{\delta}_n(t)$, (**b**) $\boldsymbol{v}_n(t)$, (**c**) $\boldsymbol{u}_{2,3}(t)$ and (**d**) $T(t)$ in a simultaneous two-point impact of a rod for the case of pure downwards translation. Stiffness values: $k_1 = k_2 = 10^8$ N/m

velocities (Fig. 2(b)) at the contact points take exactly the same values during the whole interval regardless the k values. This is not surprising: changing the stiffness results into different eigenfrequencies but does not modify the eigenmodes. Thus, only the time microscale is altered. As the impact duration and the indentation values are irrelevant and somehow arbitrary, dimensionless time and displacement scales will be used from now on.

It is worth pointing out that Newton's hypothesis is not fulfilled in that first case (though the overall process is not dissipative). The impact starts simultaneously in both points, but that in point Q_1 ends roughly at $t \approx 0.25$ ms while that at point Q_2 ends at $t \approx 0.27$ ms. In other words, collisions *overlap* (that is, the colliding points are simultaneously active) in the interval $0 \leq t \leq 0.25$ ms. The ratio between the initial approaching velocity and the final separating one (when the impact at the considered point is just over) is not equal to one:

$$\left|v_n(\mathrm{Q}_1, t \approx 0.25\ \mathrm{ms})\right| > \left|v_n(\mathrm{Q}_1, t = 0)\right|; \qquad \left|v_n(\mathrm{Q}_2, t \approx 0.27\ \mathrm{ms})\right| < \left|v_n(\mathrm{Q}_2, t = 0)\right| \tag{6.1}$$

In order to explore the system sensitivity to perturbations in the initial configuration, a second case has been calculated with the same initial velocities (pure vertical translation) but slightly different initial normal displacements ($\delta_n^-(\mathrm{Q}_1) > 0$, $\delta_n^-(\mathrm{Q}_2) = 0$). The results are shown in Fig. 3 (left column). The time and indentation scales have been normalized to the impact duration and maximum absolute value of the normal displacement of case shown in the right column in Fig. 3.

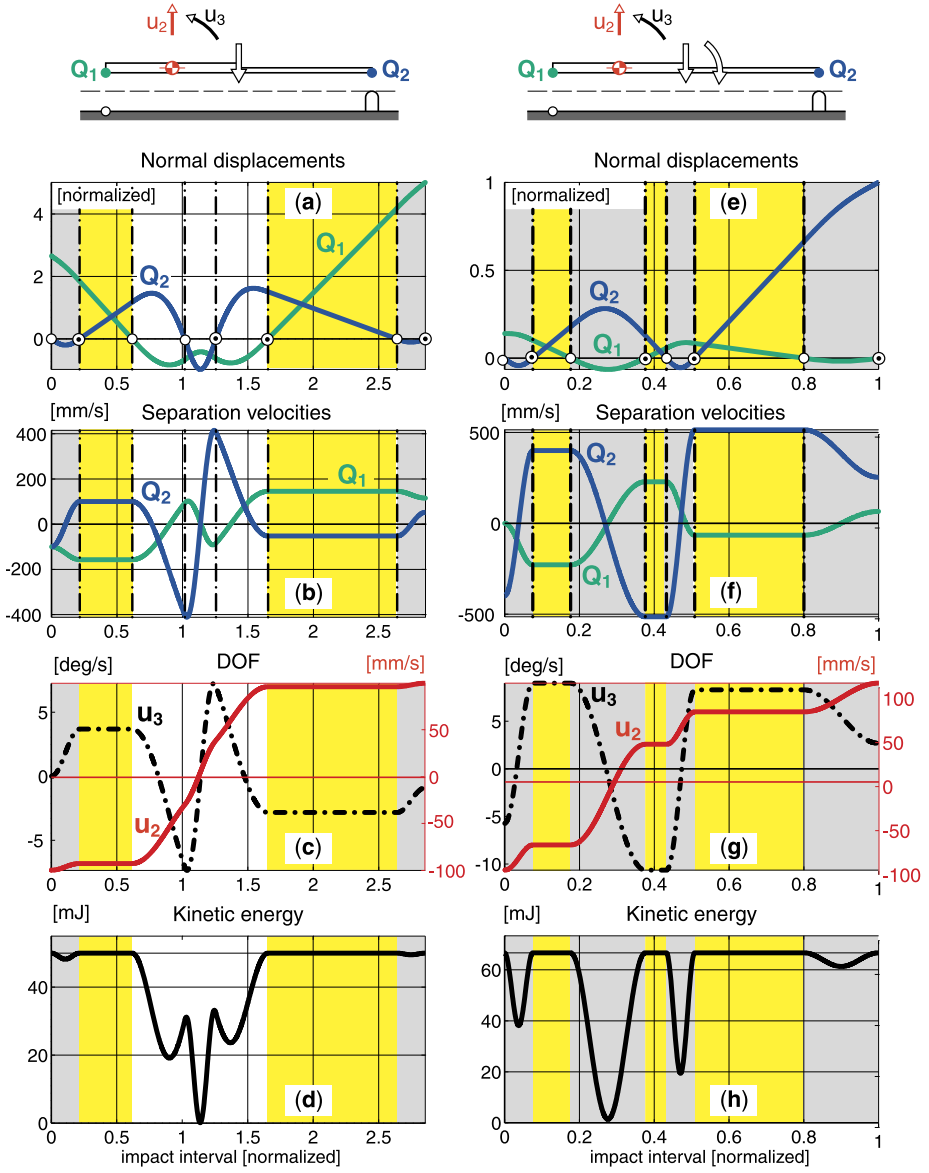

Fig. 3 Evolution of (**a**, **e**) $\boldsymbol{\delta}_n(t)$, (**b**, **f**) $\boldsymbol{v}_n(t)$, (**c**, **g**) $\boldsymbol{u}_{2,3}(t)$ and (**d**, **h**) $T(t)$ in a two-point impact of a rod for two different sets of initial conditions. Stiffness ratio $k_1/k_2 = 1$. Time and indentation scales normalized to the impact duration and maximum absolute value of the normal displacement of case shown in the right column. *Yellow shaded areas* correspond to free motion phases, grey ones to complete single-point impacts. *Right column*: Impacts show no overlapping

While for the case in Fig. 2 the impacts at points Q_1 and Q_2 showed overlapping in approximately 90 % of the impact interval (thus leading to a final state that would never be obtained if assuming sequential single-point impacts), this is not so in the two cases shown in Fig. 3. For an initial pure downwards translation (Figs. 3(a) to 3(d)), the impact starts

Table 1 Initial conditions, stiffness ratios, and final velocities of the rod colliding points

	Initial conditions		Stiff. ratio	Final vels. $[\frac{\text{mm}}{\text{s}}]$
Fig.	$\{\delta_n^-(\text{Q}_1), \delta_n^-(\text{Q}_2)\}$	$\{u_1 \quad u_2 \quad u_3\}$	k_1/k_2	$\{v_n^+(\text{Q}_1), v_n^+(\text{Q}_2)\}$
2	$\{0 \quad 0\}$	$\{0 \quad -0.1\ \frac{\text{m}}{\text{s}} \quad 0\}$	1	$\{113.10 \quad 59.49\}$
3(a) to 3(d)	$\{35\ \mu\text{m} \quad 0\}$	$\{0 \quad -0.1\ \frac{\text{m}}{\text{s}} \quad 0\}$	1	$\{121.54 \quad 32.04\}$
3(e) to 3(h)	$\{25\ \mu\text{m} \quad 0\}$	$\{0 \quad -0.1\ \frac{\text{m}}{\text{s}} \quad -0.1\ \frac{\text{rad}}{\text{s}}\}$	1	$\{65.31 \quad 253.06\}$

with a first complete short single-point impact collision (that is, ending before the other point touches the ground), where Q_2 is the only active point, followed by a free motion phase (that is, without ground contact). The coupling between points Q_1 and Q_2 is responsible for a second single point impact starting at roughly 17 % of the total impact duration. Point Q_2 collides again before Q_1 finishes the expansion phase, and so overlapping appears. A second free-motion phase appears once the impact at Q_1 is over. Though the final phase is again a single-point impact, the overlapping appearing at about a 35 % of the total interval is responsible for a final state different from the one that would be obtained without any overlapping.

The two free-motion phases can be easily identified on the DoF evolution (Fig. 3(c)): having lost the ground contact, no forces are exerted on the system and thus its DoF remain constant. Those free phases can also be identified from the other plots in the following way:

- Displacement plot (Fig. 3(a)): all points show positive displacements.
- Velocity plots (Fig. 3(b)): all points show constant normal velocity.
- Energy plots (Fig. 3(d)): the kinetic energy remains constant.

A different set of initial velocities (pure vertical downwards translation plus clockwise rotation) has been explored for the case of nonsimultaneous initial impacts (Figs. 3(e) to 3(h)). Unlike the first explored case with simultaneous initial impacts (Fig. 2), the one shown in Figs. 3(e) to 3(h) does not show overlapping at all: it is a sequence of pure complete single-point impacts. As in that case we are dealing with elastic single-point impacts on a smooth surface, the results for each complete single-point impact could be obtained analytically by means of Newton's rule with a restitution coefficient equal to one. Thus, for any impact in the sequence, $v_n^+ = v_n^-$ for the colliding point, though in general $v_n^+ \neq v_n^-$ for the noncolliding point.

All the cases presented here correspond to elastic impacts. Thus, all show a final kinetic energy equal to the initial one. However, its evolution is different according to the impact phases. Table 1 summarizes the initial conditions, the stiffness ratios and the final normal separation velocities for the different cases plotted in Figs. 2 and 3.

6.2 Example II: five-point frictionless impact of a single rigid body

The second application example consists on a five-point elastic impact of the same rod on the fixed ground, as shown in Fig. 4. The Jacobian matrix $\mathbf{A}$ relating the normal velocities of the five contact points $v_n(\text{Q}_i)$ with the degrees of freedom $\boldsymbol{u}$ (same as those defined in Fig. 1) is

$$\boldsymbol{v}_n = \mathbf{A}\boldsymbol{u} = \begin{bmatrix} 0 & 1 & -L \\ 0 & 1 & -L/2 \\ 0 & 1 & 0 \\ 0 & 1 & L \\ 0 & 1 & 3L \end{bmatrix} \begin{Bmatrix} u_1 \\ u_2 \\ u_3 \end{Bmatrix}. \tag{6.2}$$

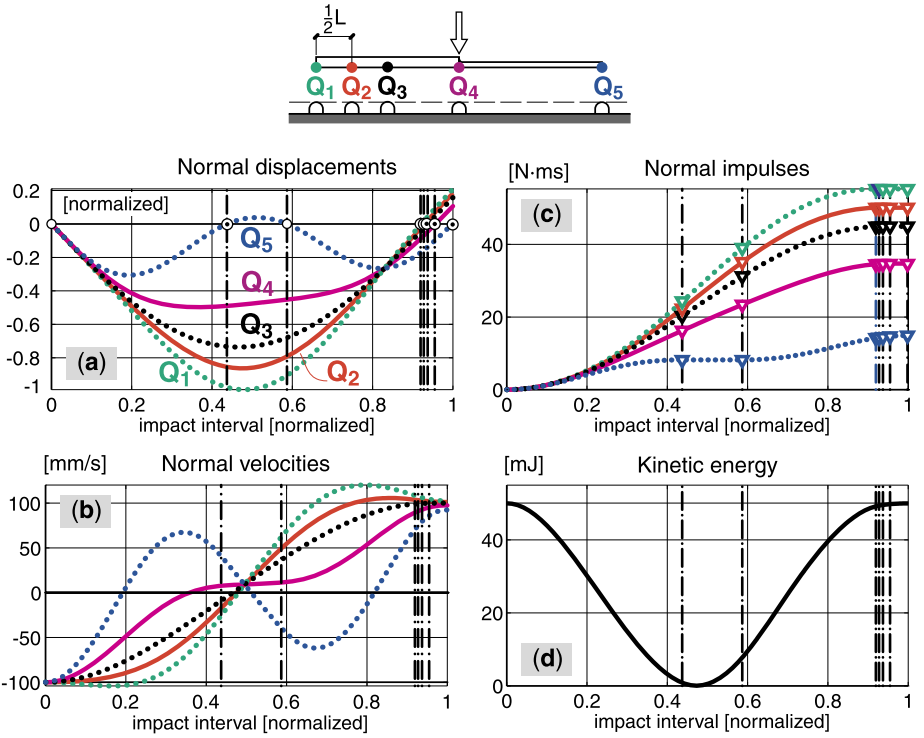

Fig. 4 Evolution of (**a**) $\boldsymbol{\delta}_n(t)$, (**b**) $\boldsymbol{v}_n(t)$, (**c**) $\boldsymbol{P}_n(t)$ and (**d**) $T(t)$ in a simultaneous five-point impact of a rod for the case of a pure downwards translation. Equal stiffness at all points. Time and indentation scales autonormalized

As $\text{rank}(\mathbf{A}) = 2 < 5$, there is redundancy. In this particular example, any pair of contact points can be chosen as independent.

Two different sets of initial velocities have been explored. The initial configuration is always horizontal, so the five points are initially in contact with the ground (no offsets are considered in the initial normal displacements). However, their initial colliding state (active/passive) depends on the initial velocities. Different stiffness ratios have also been considered.

Equal stiffness at all points is considered in the case illustrated in Fig. 4 (initial vertical translation) while Fig. 5 illustrates the effect of different stiffness at different contact points. All this information is summarized in Table 2.

We have run our simulations for different sets of independent points in order to check that the results are the same and do not depend on the particular choice of independent points. However, just one simulation per initial condition will be shown.

For the same reasons explained in the first example, dimensionless time and displacement scales have been used in Fig. 4. In this case, an "autonormalization" has been applied: the unit value in the time and the indentation scales have been associated to the impact total duration and to the maximum absolute value of the normal displacements, respectively.

The two independent points have been chosen differently for each case. Their corresponding normal displacements, velocities, and impulses are plotted in continuous line whereas those corresponding to the dependent ones are discontinuous. The incremental val-

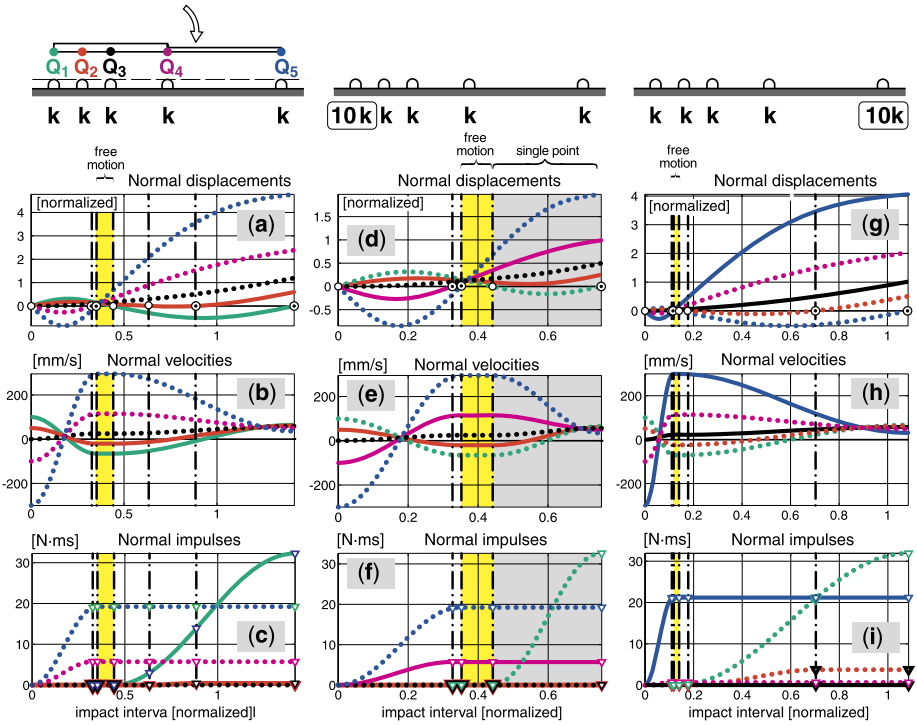

Fig. 5 Evolution of (**a**, **d**, **g**) $\boldsymbol{\delta}_n(t)$, (**b**, **e**, **h**) $\boldsymbol{v}_n(t)$ and (**c**, **f**, **i**) $\boldsymbol{P}_n(t)$ in a five-point impact of a rod for the case of clockwise rotation. Equal stiffness at all points (**a**, **b**, **c**), Q_1 stiffness ten times higher (**d**, **e**, **f**), Q_5 stiffness ten times higher (**g**, **h**, **i**). *Continuous/discontinuous lines* correspond to independent/redundant points. Time and indentation scales normalized according to the unit values used in Fig. 4. *Yellow shaded areas* correspond to free motion phases, grey ones to complete single-point impacts

Table 2 Initial conditions and stiffness of the rod-ground contact at the colliding points

Fig.	Initial conditions $\{u_1 \quad u_2 \quad u_3\}$	Initial colliding state of points a/p = active/passive	Points stiffness $(k_1, k_2, k_3, k_4, k_5)$
4	$\{0 \quad -0.1\,\frac{\text{m}}{\text{s}} \quad 0\}$	(a, a, a, a, a)	$(1, 1, 1, 1, 1) \times 10^{15}\,\frac{\text{N}}{\text{m}}$
5	$\{0 \quad 0 \quad -0.1\,\frac{\text{rad}}{\text{s}}\}$	(p, p, p, a, a)	Left: $(1, 1, 1, 1, 1) \times 10^{15}\,\frac{\text{N}}{\text{m}}$ Middle: $(10, 1, 1, 1, 1) \times 10^{15}\,\frac{\text{N}}{\text{m}}$ Right: $(1, 1, 1, 1, 10) \times 10^{15}\,\frac{\text{N}}{\text{m}}$

ues of the impulses, calculated as explained in Sect. 6, are indicated with a small triangle superposed to the impulses evolution (obtained through time integration of the indentations).

Figure 4 shows a simultaneous five-point impact with initial downwards translation and unit stiffness ratios ($k_i/k_j = 1, \forall(i, j)$). Point Q_5 displacement curve (Fig. 4(a), blue line) presents an intermediate positive phase (with duration roughly a 15 % of the whole impact interval), which indicates that its colliding state is passive. Consequently, no normal impulse is generated at Q_5 within that impact subinterval, and the corresponding impulse curve (Fig. 4(c)) remains horizontal. Different short phases appear toward the end of the

whole interval, each one corresponding to a new point switching from active to passive state.

Finally, Fig. 5 shows three cases with identical initial conditions (and so identical initial colliding states for all points) but different stiffness coefficients. Plots from (a) to (c) correspond to equal points stiffness, whereas those from (d) to (f) and from (g) to (i) correspond to $(k_1/k_{2\to5}) = 10$ and $(k_5/k_{1\to4}) = 10$, respectively. The time and indentation scales have been normalized according to the unit values used in Fig. 4.

For the case of equal stiffness (Figs. 5(a) to 5(c)), the higher impulse is generated at point Q_1, which is coherent with the fact that the negative area defined by the normal displacement and the time axis (upper left plot) is higher for that point than for the others.

In the case where $k_1/k_{i\neq1} = 10$ (Figs. 5(d) to 5(f)), two points (Q_2 and Q_3) are permanently passive, and so do not develop any normal impulse. The higher impulse corresponds again to point Q_1, though its indentation curve defines a lower negative area than that of the other two active points: the higher value of k_1 compensates for this low area value.

When the stiffer point is Q_5 (Figs. 5(g) to 5(i)), the higher impulse is again that generated at point Q_1: though k_5 is ten times higher than k_1, the negative normal displacement of point Q_1 attains a maximum absolute value double than that of point Q_5, and spreads along roughly 90 % of the whole interval, while that of point Q_5 is concentrated in the first 10 %.

6.3 Example III: three-point frictionless impact of a two-link chain

Figure 6 corresponds to multiple-point impacts of a simple multibody system (a two-link chain). Table 3 summarizes the initial conditions and the stiffness values of all the explored cases. Autonormalization has been applied to all time and indentation scales.

The colliding points have been chosen so that two of them (Q_1 and O) are "conjugate percussion centers": if the right segment has no contact with the ground, impulses at Q_1(O) generate neither a velocity change nor a constraint impulse at point O(Q_1). However, if there is ground contact at points located on the right segment (S_1, S_2, and S_3), impulses at those points do generate impulses at O.

In the two cases shown in Figs. 6(a) to 6(c) and Figs. 6(d) to 6(f), the right segment does not touch the ground, impulses generated at Q_1 will not have any consequence on O.

Some perturbations (small enough) on the ground profile have been added in order to have nonsimultaneous impacts: first point Q_1 collides, then eventually points Q_2 and O (one after the other) or just point O, depending on the initial conditions and the ground stiffness.

In both cases, as the impact starts at Q_1, no impulsive forces are transmitted to the right segment through O until point Q_2 starts colliding with the ground. Consequently, the right-segment motion is uniform, and v_n(O) is constant until that second impact starts.

For the particular case of "hard ground" (stiffness $10k$, left column), impact at Q_1 is over before that at Q_2 starts. Thus, during the subinterval defined by those two conditions the

Table 3 Initial conditions and stiffness of the rods-ground at the colliding points

Fig.	Initial conditions $\{u_1 \quad u_2 \quad u_3 \quad u_4\}$	Initial colliding state of points a/p = active/passive	Ground stiffness
6(a) to 6(c)	$\{0 \quad -1\ \frac{\text{m}}{\text{s}} \quad 0 \quad 40\ \frac{\text{deg}}{\text{s}}\}$	(a, p, p)	$10k$
6(d) to 6(f)	$\{0 \quad -1\ \frac{\text{m}}{\text{s}} \quad 0 \quad 40\ \frac{\text{deg}}{\text{s}}\}$	(a, p, p)	k
6(g) to 6(i)	$\{0 \quad -1\ \frac{\text{m}}{\text{s}} \quad 0 \quad 40\ \frac{\text{deg}}{\text{s}}\}$	(a, a, a, p, p, p)	k

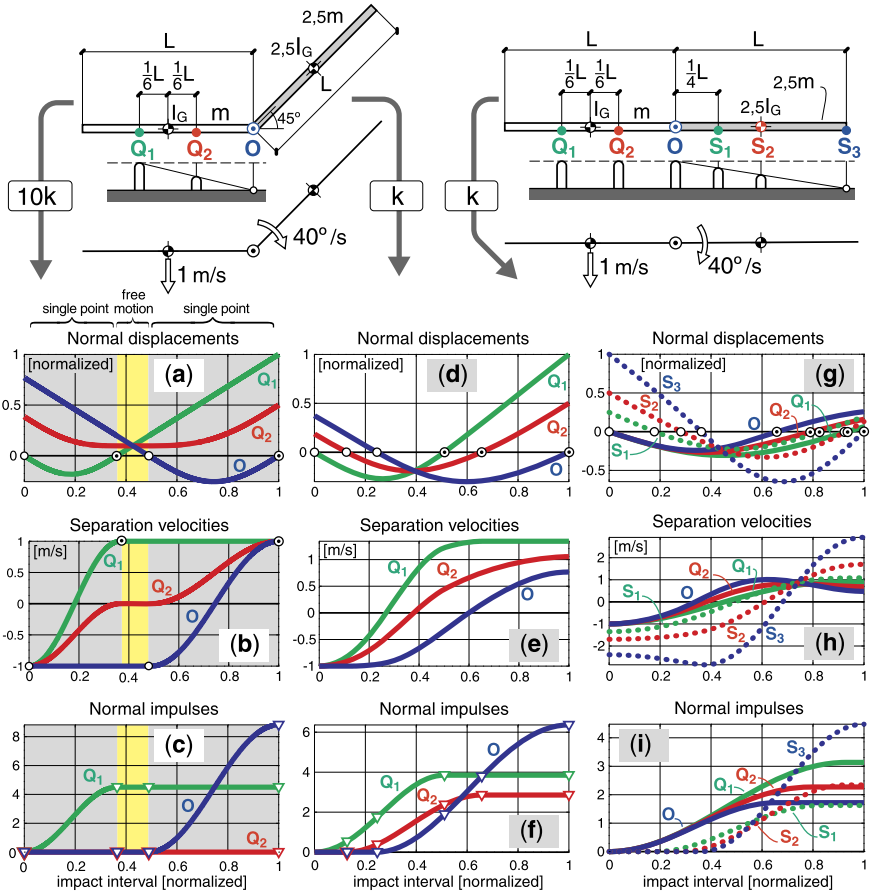

Fig. 6 Evolution of (**a**, **d**, **g**) $\boldsymbol{\delta}_n(t)$, (**b**, **e**, **h**) $\boldsymbol{v}_n(t)$ and (**c**, **f**, **i**) $\boldsymbol{P}_n(t)$ in a three-point (**a**, **b**, **c**; **d**, **e**, **f**) and a six-point (**g**, **h**, **i**) impact of a two-link chain. Initial state described in the upper pictures. Equal stiffness k is considered at all points in cases (**d**, **e**, **f**; **g**, **h**, **i**) while a higher value ($10k$) at all points is considered in case (**a**, **b**, **c**). *Continuous/discontinuous lines* correspond to points located on the left/right segment. Time and indentation scales autonormalized. *Yellow shaded areas* correspond to free motion phases, grey ones to complete single-point impacts

system evolves freely (yellow shaded area), and the velocity of all points remains constant. As impacts do not overlap, Newton's rule is fulfilled for each impact.

The final value of the normal impulse generated at point O is higher than that at point Q_1, which is consistent with the higher indentation and longer impact at O as compared to those at Q_1.

In the case shown in Figs. 6(d) to 6(f), the softer ground (only k instead of $10k$) is responsible now for the overlapping of impacts at all impact points. Newton's rule does not apply any more.

6.4 Example IV: six-point frictionless impact of a two-link chain

A final case is presented in Figs. 6(g) to 6(i). A soft ground is considered and some perturbations (small enough) on the ground profile have been added in order to have non-

simultaneous impacts: first points Q_1, Q_2, and O collide simultaneously, then eventually points S_1 to S_3 (one after the other), depending on the initial conditions and the ground stiffness.

The main interest of this example is that of including a case dealing with a multibody system with redundancy (none of the previous examples had these two characteristics). Being a more complicated example, it is difficult to do any comments based on predictable motion features.

The total impact interval consists on a succession of eight phases where the points colliding states ("a" for active, "p" for passive) are the following:

$$(a, a, a, p, p, p) \rightarrow (a, a, a, a, p, p) \rightarrow (a, a, a, a, a, p) \rightarrow (a, a, a, a, a, a) \rightarrow (a, a, p, a, a, a)$$

$$\rightarrow (a, p, p, a, a, a) \rightarrow (a, p, p, p, a, a) \rightarrow (a, p, p, p, p, a) \rightarrow (p, p, p, p, p, a)$$

$$\rightarrow (p, p, p, p, p, p)$$

No single-point impact phases appear or, what is the same, impact overlapping spreads throughout the impact interval. Consequently, Newton's rule does not apply.

7 Conclusions

A simple linear-by-part vibrational approach has been presented to study both nonredundant and redundant perfectly elastic frictionless multiple-point impacts in multibody systems with perfect constraints.

The approach assumes a constant system configuration as far as the system inertia and Jacobian matrices are concerned, and so, in this respect, it is close to impulsive approaches. Nevertheless, it assumes continuous vibrational linear dynamics at the colliding points, with a convenient time scale in order to be consistent with the system constant configuration assumption.

At each time instant (in the microscale), the chosen set of independent contact points defines a collection of vibration modes, which allow to keep track, in a simple analytical way, of the normal velocities and displacements of the full set of contact points.

A characteristic feature of the approach is the use of a reduced inertia matrix associated with the contact points. For the case of nonredundant impacts, the dimension of the reduced inertia matrix is equal to the number of contact points, regardless the number of DoF exhibited by the system. That matrix is obtained by means of a physically meaningful decomposition of the system kinetic energy into that associated with the motion in the normal directions at the contact points, and that associated with motion compatible with zero normal velocities.

For the case of redundant impacts, the reduced inertia matrix is associated with just the chosen independent points in the contact space. The mechanical state of the redundant contact points is obtained from the independent ones through the redundancy matrix.

At each active point, the contact between bodies is modeled through a linear normal stiffness, high enough to neglect changes in the inertia matrix. The set of active points may change along the process, and consequently the set of springs to be considered and the resulting stiffness matrix used in the vibrational formulation have to be modified accordingly. That matrix is associated with all the active contact points in all cases. For the case of nonredundant impacts, the stiffness matrix is always diagonal, whereas this is not the case if redundancy appears.

As the normal forces at the contact points are formulated from the normal displacements, the approach retains the high sensitivity of multiple-point impacts to changes in the initial

configuration. Small perturbations of the initial configuration may lead to a quite different evolution of the normal forces, and consequently, of the system final velocities.

In order to obtain the individual values of the normal impulses generated at each colliding point, it is possible either to integrate the normal displacements at each point (once the vibrational problem has been solved) or use an algebraic formulation allowing the calculation of the incremental impulses at each impact phase. In that case, only the active points are taken into account.

All the application examples show the capacity of the approach to retain the high sensitivity to initial conditions without assuming particular sequences of single point impacts, as is usually done in impulsive approaches, and without the time consuming integration process that would require the use of the nonlinear contact stiffness Hertz model. For systems with a high number of DoF, the presented approach is also less time consuming than that of a vibratory linear model directly associated with the system original inertia matrix (without reduction).

References

1. Schiehlen, W., Seifried, R., Eberhard, P.: Elastoplastic phenomena in multibody impact dynamics. Comput. Methods Appl. Mech. Eng. **195**, 6874–6890 (2006). doi:10.1016/j.cma.2005.08.011
2. Gilardi, G., Sharf, I.: Literature survey of contact dynamics modelling. Mech. Mach. Theory **37**, 1213–1239 (2002). doi:10.1016/S0094-114X(02)00045-9
3. Agulló, J., Barjau, A.: Rough impacts in multibody systems. Mech. Mach. Theory **26**(6), 565–577 (1991). doi:10.1016/0094-114X(91)90039-7
4. Liu, C., Zhao, Z., Brogliato, B.: Frictionless multiple impacts in multibody systems. I. Theoretical framework. Proc. R. Soc. A, Math. Phys. Eng. Sci. **464**, 3193–3211 (2008). doi:10.1098/rspa.2008.0078
5. Newby, N.D.: Linear impacts with harmonic oscillator forces: the inverse scattering forces. Am. J. Phys. **47**(2), 161–165 (1979)
6. Acary, V., Brogliato, B.: Concurrent multiple impacts modelling: case study of a 3-ball chain. In: Bathe, K.J. (ed.) Proc. MIT Conf. on Computational Fluid and Solid Mechanics, pp. 1836–1841. Elsevier Science, Amsterdam (2003)
7. Acary, V., Taha, D.E.: Concurrent multiple impacts in rigid bodies: formulation and simulation. In: Fifth Euromech Nonlinear Dynamics Conference, ENOC, Eindhoven University of Technology, Eindhoven, Pays-Bas. Springer, Berlin (2005)
8. Jia, Y.-B., Mason, M.T., Erdmann, M.A.: Multiple impacts: a state transition diagram approach. Int. J. Robot. Res. **32**(1), 84–114 (2013). doi:10.1177/0278364912461539
9. Yilmaz, C., Gharib, M., Hurmuzlu, Y.: Solving frictionless rocking block problem with multiple impacts. Proc. R. Soc. A **465**, 3323–3339 (2009). doi:10.1098/rspa.2009.0273
10. Poisson, S.D.: Traité de Mécanique. Bachelier, Imprimeur, vol. 2. Librairie, Paris (1983)
11. Delunay, Ch.: Traité de Mécanique Rationelle. Livre IV: Dinamique, troisième partie. Langlois and Leclerq, Victor Masson, Paris (1856)
12. Résal, H.: Traité de Mecanique Générale. Tome VII: Développements sur la Mécanique Rationelle et la Cinématique Pure. Gautier-Villars, Paris (1889)
13. Boulanger, G.: Note sur le choc avec frottement des corps non parfaitement élastiques. Rev. Sci. **5**, 325–327 (1939)
14. Brogliato, B.: Nonsmooth impact mechanics: models, dynamics and control. In: Lecture Notes in Control and Information Sciences, p. 220. Springer, Berlin (1996)
15. Stronge, W.J.: Impact Mechanics. Cambridge University Press, Cambridge (2000)
16. Brogliato, B., Zhang, H., Liu, C.: Analysis of a generalized kinematic impact law for multibody-multicontact systems, with application to the planar rocking block and chains of balls. Multibody Syst. Dyn. **27**, 351–382 (2012). doi:10.1007/s110044-012-9301-3
17. Batlle, J.A.: On Newton's and Poisson's rules of percussive dynamics. J. Appl. Mech. **60**, 376–381 (1993). doi:10.1115/1.2900804
18. Bowling, A., Flickinger, D.M., Harmeyer, S.: Energetically consistent simulation of simultaneous impacts and contacts in multibody systems with friction. Multibody Syst. Dyn. **22**, 27–45 (2009). doi:10.1007/s511044-009-9147-5

19. Ruspini, D.C., Khatib, O.: Impact/contact models for the dynamic simulation of complex environments. In: Proc. IEEE/RSJ Int. Conf. on Intelligent Robots and Systems (1997)
20. Mirtich, B., Canny, J.: Impulse-based simulation of rigid bodies. In: Proc. of the 1995 Symposium on Interactive 3D Graphics (1995). doi:10.1145/199404.199436
21. Glocker, C., Pfeiffer, F.: Multiple impacts with friction in rigid multibody systems. J. Nonlinear Dyn. **7**, 471–497 (1995). doi:10.1007/BF00121109
22. Caselli, F., Frémond, M.: Impact of three balls on a plane. Comput. Mech. **43**, 743–754 (2009). doi:10.1007/s00466-008-0342-7
23. Johansson, L.: A Newton method for rigid body frictional impact with multiple simultaneous impact points. Comput. Methods Appl. Mech. Eng. **191**, 239–254 (2001). doi:10.1016/S0045-7825(01)00272-9
24. Ruspini, D.C., Khatib, O.: A framework for multi-contact multi-body dynamic simulation and haptic display. In: Proc. IEEE/RSJ Int. Conf. on Intelligent Robots and Systems, vol. 2, pp. 1322–1327 (2000). doi:10.1109/IROS.2000.893204
25. Moreau, J.J.: Some numerical methods in multibody dynamics: application to granular materials. Eur. J. Mech. A, Solids **13**(4), 93–114 (1994)
26. Kövecses, J.: Dynamics of mechanical systems and the generalized free-body diagram—part I: general formulation. J. Appl. Mech. **75**, 061012 (2008). doi:10.1115/1.2965372
27. Constantinescu, D., Salcudean, S.E., Croft, E.A.: Haptic rendering of rigid body impacts. In: Proc. 12th Int. Symposium HAPTICS'04, pp. 2–8 (2004). doi:10.1109/HAPTIC.2004.1287171